Wind and Structures, *Vol. 17, No. 2(2013) 203-225*
DOI:http://dx.doi.org/10.12989/was.2013.17.2.203

Analysis on running safety of train on bridge with wind barriers subjected to cross wind

T. Zhang, H. Xia* and W.W. Guo

School of Civil Engineering, Beijing Jiaotong University, Beijing, 100044, China

(Received April 26, 2012, Revised September 4, 2012, Accepted December 1, 2012)

Abstract. An analysis framework for vehicle-bridge dynamic interaction system under turbulent wind is proposed based on the relevant theory of wind engineering and dynamics. Considering the fluctuating properties of wind field, the stochastic wind velocity time history is simulated by the Auto-Regressive method in terms of power spectral density function of wind field. The bridge is represented by three-dimensional finite element model and the vehicle by a multi-rigid-body system connected by springs and dashpots. The detailed calculation formulas of unsteady aerodynamic forces on bridge and vehicle are derived. In addition, the form selection of wind barriers, which are applied as the windbreak measures of newly-built railways in northwest China, is studied based on the suggested evaluation index, and the suitable values about height and porosity rate of wind barriers are studied. By taking a multi-span simply-supported box-girder bridge as a case study, the dynamic response of the bridge and the running safety indices of the train traveling on the bridge with and without wind barriers are calculated. The limit values of train speed with respect to different wind velocities are proposed according to the allowance values in the design code.

Keywords: wind-train-bridge coupled system; turbulent wind field; wind barrier; unsteady aerodynamic force; running safety of train

1. Introduction

Strong wind happens frequently in Xinjiang and coastal regions in China where the maximum mean wind velocity even exceeds 40 m/s. There have been many overturn accidents of highway and railway vehicles caused by strong wind, which leads to enormous disaster. For example, on the existed Lanzhou-Xinjiang railway in China, more than 30 derailment and rollover accidents of train have happened and about 100 vehicles been flipped by strong wind since the railway opened (Qian 2009). The overturn accidents were often reported in news reports during the typhoon seasons in coastal areas. The wind-induced accidents of vehicles also occurred occasionally in other countries, such as in 1981 in India, a passenger train was blown down from the bridge that caused above 800 deaths; and in Japan, wind is said to have caused at least 29 derailments (Liu *et al.* 2008) since 1872 when its transport service was open.

The strong wind may produce a serious threat to the safety of railway and cause significant

*Corresponding author, Professor, E-mail: hxia88@163.com

http://www.techno-press.org/?journal=was&subpage=8 ISSN: 1226-6116 (Print), 1598-6225 (Online)

economic losses, so effective measures should be taken to ensure the safety of running trains. There are two ways to prevent a train from overturn: one is to reduce the aerodynamic rolling moment acting on its vehicles, another is to stop the train when the wind velocity exceeds the limit value. The first way involves installation of wind barriers, and the second way involves wind velocity monitoring and use of train operation control. The experience of Japan's Shinkansen shows that installation of wind barrier can obviously decrease the number of train stops under strong wind (Noguchi *et al*. 2000, Fujii *et al*. 1999). Therefore, it is necessary and effective to set wind barriers on bridges in strong wind field, to ensure the running safety and stability of train.

The existed research mainly concentrated on the identification of aerodynamic parameters of bridges from the wind tunnel test or in-site measurement (Han *et al*. 2010, Nikitas *et al*. 2011), and the wind-induced vibration analysis of large span bridges, including the buffeting, flutter, vortex-excited vibration and wind-rain vibration of bridges (Xiang *et al*. 2005, Zhang *et al*. 2011, Zhang 2011), the train-bridge coupling vibration (Li and Zhu 2010) and the aerodynamic properties and running safety of trains in strong wind field (Li *et al*. 2005, Chen *et al*. 2010). There have been many research results on wind-induced instability of vehicles on roads without wind barriers (Wetzel *et al*. 2008, Orellano *et al*. 2002, Diedrichs *et al*. 2007 and 2010, Cooper *et al*. 1979, Carrarini 2007, Andersson *et al*. 2004) and on the aerodynamic characteristic of different vehicles on embankments or bridges under cross winds adopting numerical simulation and wind tunnel test method (Ahmed *et al*. 1985, Cheli *et al*. 2003, Cooper 1981, Howell 1986, Suzuki *et al*. 2003). Some efforts were also made to improve the protection, as the vehicles are extremely exposed to strong wind gusts (Baker *et al*. 1992, Saito *et al*. 2006). Strukelj *et al*. (2005) numerically studied the effects of wind barrier geometry on resulting wind forces on vehicles. They also tested a part of barrier prototype in the wind tunnel in terms of thermal and mechanical endurance. While usually very helpful for improving traffic safety, wind barriers have negative influence on aerodynamic characteristics of bridge itself. In fact, windbreaks are used all over the world for purposes such as reduction of soil erosion, control of snowdrift and provision of a favorable microclimate for humans, animals and plants. Many studies can be found on the change of flow through windbreak structures (Wilson 1985, Hagen *et al*. 1981, Heisler *et al*. 1988). For the wind barriers on bridges, Procino *et al*. (2008) investigated the possibilities of protecting the vehicles on highway viaducts and the effects of wind barrier porosity on a flow field by wind tunnel tests. Furthermore, Kwon *et al*. (2011) and Kim *et al*. (2011) presented the design criteria required for wind barriers to protect vehicles running on an expressway under a high side wind and a decision-making process for installation of wind barriers. However, the above-mentioned studies on wind barriers were aimed at the highway bridges, while for railway bridges, the research on the interaction between wind barriers and running trains has been given little attention.

In this paper, an analysis model for vehicle-bridge dynamic interaction under turbulent wind is established, and the calculation formula of unsteady aerodynamic forces on bridge and vehicle are derived. Then the form selection of wind barriers is studied using the CFD software, based on which the suggested index for evaluating windbreak effect of wind barriers and the reasonable height and porosity rate of wind barriers are given. Finally, taking an actual bridge for example, the dynamic response of the bridge and the running safety indices of the train passing the bridge with and without wind barriers are calculated. The limit values of train speed with respect to different wind velocities are proposed according to the allowance values in the design code.

2. Wind-field model and wind force computation

2.1 Simulation of turbulent wind-field

An autoregressive model can be used to simulate the wind velocity field, as it is essentially stochastic time series. In an AR (Auto-Regressive) model, the *m*-th related turbulent wind time histories $\mathbf{v}(\mathbf{X}, \mathbf{Y}, \mathbf{Z}, t)=[v_1(x_1, y_1, z_1, t)\ v_2(x_2, y_2, z_2, t)\ \ldots v_m(x_m, y_m, z_m, t)]$ can be generated by

$$\mathbf{v}(\mathbf{X}, \mathbf{Y}, \mathbf{Z}, t) = -\sum_{n=1}^{p} \boldsymbol{\varphi}_n \cdot \mathbf{v}(\mathbf{X}, \mathbf{Y}, \mathbf{Z}, t - n \cdot \Delta t) + \mathbf{N}(t) \tag{1}$$

where: $\mathbf{X}=[x_1, x_2, \ldots, x_m]^T$, $\mathbf{Y}=[y_1, y_2, \ldots, y_m]^T$, $\mathbf{Z}=[z_1, z_2, \ldots, z_m]^T$, (x_i, y_i, z_i) is the coordinate of the *i*-th point, *i* = 1, 2, 3, …, *m*; *p* is the order of the AR model, which is selected according to FPE (Final Prediction Error) criterion and AIC (Akaike Information Criterion) (Zhang *et al*. 2012); Δt is the time interval of wind field simulation; $\boldsymbol{\varphi}_n$ is the autoregressive coefficient $m \times m$ square matrix of the AR model, *n*= 1, 2, …, *p*; $\mathbf{N}(t)$ is a zero-mean independent stochastic process with given variance.

For convenience, $\mathbf{v}(\mathbf{X}, \mathbf{Y}, \mathbf{Z}, t)$ is written as $\mathbf{v}(t)$. Based on the assumption of wind field simulation and the characteristics of auto-correlation function expressed by Eqs. (2) and (3), the relationship between the correlations function $\mathbf{R}(j \cdot \Delta t)$ and the autoregressive coefficient $\boldsymbol{\varphi}_n$ is given by

$$\mathbf{R}(-j \cdot \Delta t) = \mathrm{E}\left[\mathbf{v}(t) \cdot \mathbf{v}^{\mathrm{T}}(t - j \cdot \Delta t)\right] \tag{2}$$

$$\mathbf{R}(-j \cdot \Delta t) = \mathbf{R}(j \cdot \Delta t) \tag{3}$$

$$\mathbf{R}(j \cdot \Delta t) = -\sum_{n=1}^{p} \boldsymbol{\varphi}_n \cdot \mathbf{R}[(j - n) \cdot \Delta t], \quad j=1, 2, \ldots, p \tag{4}$$

$$\mathbf{R}(0) = -\sum_{n=1}^{p} \boldsymbol{\varphi}_n \cdot \mathbf{R}(n \cdot \Delta t) + \mathbf{R}_N \tag{5}$$

Eqs. (4) and (5) can be expressed with a matrix form as follows

$$\mathbf{R} \cdot \boldsymbol{\varphi} = \begin{bmatrix} \mathbf{R}_N \\ \mathbf{O}_p \end{bmatrix} \tag{6}$$

where $\boldsymbol{\varphi}_{(p+1)m \times m} = [\mathbf{I}\ \ \boldsymbol{\varphi}_1\ \ \boldsymbol{\varphi}_2\ \ \cdots\ \ \boldsymbol{\varphi}_p]^{\mathrm{T}}$, $\mathbf{I}$ is the *m* order unit matrix; $\mathbf{R}_N$ is the $m \times m$ covariance matrix; $\mathbf{O}_p$ is a $pm \times m$ matrix where all elements are zero; $\mathbf{R}$ is $(p+1)m \times (p+1)m$ auto-correlation Toeplitz matrix, and the detailed expression is

$$\mathbf{R} = \begin{bmatrix} \mathbf{R}_{11}(0) & \mathbf{R}_{12}(\Delta t) & \mathbf{R}_{13}(2\Delta t) & \cdots & \mathbf{R}_{1(p+1)}(p\Delta t) \\ \mathbf{R}_{21}(\Delta t) & \mathbf{R}_{22}(0) & \mathbf{R}_{23}(\Delta t) & \cdots & \mathbf{R}_{2(p+1)}[(p-1)\Delta t] \\ \mathbf{R}_{31}(2\Delta t) & \mathbf{R}_{32}(\Delta t) & \mathbf{R}_{33}(0) & \cdots & \mathbf{R}_{3(p+1)}[(p-2)\Delta t] \\ \vdots & \vdots & \vdots & \ddots & \vdots \\ \mathbf{R}_{(p+1)1}(p\Delta t) & \mathbf{R}_{(p+1)2}[(p-1)\Delta t] & \mathbf{R}_{(p+1)3}[(p-2)\Delta t] & \cdots & \mathbf{R}_{(p+1)(p+1)}(0) \end{bmatrix}_{(p+1)m \times (p+1)m} \tag{7}$$

in which $\mathbf{R}_{sd}(j\Delta t)$ is $m \times m$ square matrix (*s*=1, 2, …, *p*+1, *d*=1, 2, …, *p*+1, *j*=0, 1, 2, …, *p*) whose

elements can be calculated by the Wiener-Khintchine formula

$$R_{iq}(\tau) = \int_0^\infty S_{iq}(f)\cos(2\pi f \cdot \tau)\mathrm{d}f \tag{8}$$

where f is the frequency of fluctuating wind (Hz); if i=q, $S_{iq}(f)$ is the auto-spectral density function, else $S_{iq}(f)$ is the cross-spectral density function of fluctuating wind (i=1, 2, 3, …, m, q=1, 2, 3, …, m) that depends on the auto-spectral density function $S_{ii}(f)$, $S_{qq}(f)$ and relationship function $r_{iq}(f)$, i.e.

$$S_{iq}(f) = \sqrt{S_{ii}(f)S_{qq}(f)} \cdot r_{iq}(f) \cdot \exp[i\theta(f)] \tag{9}$$

where $\theta(f) = 0$ in terms of the assumption of wind field simulation; for the structure with large vertical and lateral size the relationship function $r_{iq}(f)$ is suggested by Davenport (1961)

$$r_{iq}(f) = \exp\left[-\frac{2f\sqrt{C_z^2(z_i - z_q)^2 + C_x^2(x_i - x_q)^2}}{\bar{v}(z_i) + \bar{v}(z_q)}\right] \tag{10}$$

where $\bar{v}(z_i)$ and $\bar{v}(z_q)$ are the mean wind velocity at the i-th and q-th point respectively; (x_i, z_i) and (x_q, z_q) are the coordinate of the i-th and q-th point respectively; C_x and C_z are the attenuation factor of any two spatial points along the x-axis and z-axis. C_x and C_z can be obtained by field test, or use the values C_x=16 and C_z=10 suggested by Simiu (1978) in actual projects if lack of measured data.

After the matrix $\mathbf{R}$ is calculated, the autoregressive coefficient $\boldsymbol{\varphi}_n$ can be obtained using Eq. (6), and the $\mathbf{R}_N$ can be solved by substituting $\boldsymbol{\varphi}_n$ into Eq. (5). In this way, the wind velocity time series can be easily generated using Eq. (1).

2.2 Numerical calculation of crosswind through wind barriers on bridge

Based on the CFD software and using the RNG k-ε turbulence model, the numerical simulation is performed for the flow field distribution through wind barriers on bridge, further the windbreak effect is analyzed of wind barriers with different heights and different porosities. The fluid motion equations are derived according to the conservation principle of mass and momentum, which are solved by the finite volume method. The computational domain is discretized with non-structural grid generation technique, which is highly adaptable, efficient and easy in fining the mesh as required.

In lateral wind-field, the bridge and wind barrier are approximated as a two-dimensional model, where the flow field is incompressible because the oncoming wind velocity is far less than 0.3 times sound velocity. The porosity of wind barriers are modeled with the gap between blocks, whose thickness is the same as that of wind barriers at the corresponding position and whose height depends on the height and porosity rate of barriers. The two-dimensional incompressible governing equations of fluid movement using tension analysis method can be expressed as (Zhou 2010)

$$\frac{\partial \bar{u}_i}{\partial x_i} = 0 \tag{11}$$

$$\frac{\partial \overline{u}_i \overline{u}_j}{\partial x_j} = -\frac{1}{\rho}\frac{\partial \overline{p}}{\partial x_i} + \nu \frac{\partial^2 \overline{u}_i}{\partial x_j \partial x_j} + \frac{\partial}{\partial x_j}\left[\nu_{\mathrm{t}}\left(\frac{\partial \overline{u}_i}{\partial x_j} + \frac{\partial \overline{u}_j}{\partial x_i}\right)\right] \tag{12}$$

$$\frac{\partial (k\overline{u}_i)}{\partial x_i} = \frac{\partial}{\partial x_j}\left[\alpha_{\mathrm{k}}(\nu_{\mathrm{t}} + \nu)\frac{\partial k}{\partial x_j}\right] + \varepsilon + P_{\mathrm{k}} \tag{13}$$

$$\frac{\partial (\varepsilon \overline{u}_i)}{\partial x_i} = \frac{\partial}{\partial x_j}\left[\alpha_{\varepsilon}(\nu_{\mathrm{t}} + \nu)\frac{\partial \varepsilon}{\partial x_j}\right] + C_{\varepsilon 1}^{*}\frac{\varepsilon}{k}P_{\mathrm{k}} - C_{\varepsilon 2}\frac{\varepsilon^2}{k} \tag{14}$$

where the cap bar "–" indicates the time average of the corresponding physical quantities; ρ is the air density; ν is the kinematic viscosity; ε is the turbulent kinetic energy dissipation rate; ν_{t} is the eddy viscosity, and P_{k} is the generated term of turbulent kinetic energy, expressed as

$$\nu_{\mathrm{t}} = C_{\nu} k^2 / \varepsilon \tag{15}$$

$$P_{\mathrm{k}} = \nu_{\mathrm{t}}\left(\frac{\partial \overline{u}_i}{\partial x_j} + \frac{\partial \overline{u}_j}{\partial x_i}\right)\frac{\partial \overline{u}_i}{\partial x_j} \tag{16}$$

where C_{ν} is the model coefficient, generally equals to 0.0845; $\alpha_{\mathrm{k}} = \alpha_{\varepsilon} = 1.39$; and $C_{\varepsilon 1}^{*}$ is related to β and η, which can be written as

$$C_{\varepsilon 1}^{*} = C_{\varepsilon 1} - \eta(1 - \eta/\eta_0)/(1 + \beta\eta^3);\quad \eta = \sqrt{2E_{ij}\cdot E_{ij}}\cdot k/\varepsilon;\quad E_{ij} = \frac{1}{2}\left(\frac{\partial \overline{u}_i}{\partial x_j} + \frac{\partial \overline{u}_j}{\partial x_i}\right)$$

where: $C_{\varepsilon 1} = 1.42$, $C_{\varepsilon 2} = 1.68$; $\eta_0 = 4.377$, $\beta = 0.012$; and E_{ij} represents the time average strain rate of main flow.

In order to ensure the accuracy of the calculation, and consider the computing capability and efficiency, the calculation region of the model should be chosen reasonably. Qu *et al.* (2007) showed that the flow field parameters near outer boundary could be greatly compatible with given boundary conditions when the size of outside boundary is greater than 20 times characteristic size of model section, and solutions have better distribution and faster convergence. In this paper, the distance from inlet boundary to the structure center is 20 times width of the model section, 25 times from outlet boundary to the structure center, and the distance from the top or bottom boundary to the structure center is greater than 20 times height of the model section. In the near wall area, the value range of y^{+} is 30 to 60, thus the grid size is calculated by $\Delta y_{\mathrm{p}} = y^{+}\mu/(\rho C_{\mu}^{1/4} k^{1/2})$, in which Δy_{p} is normal distance from the wall center element to wall surface, k is the turbulence kinetic energy of the wall center element, C_{μ} is a const depend on the turbulence model, μ is the dynamic viscosity of fluid, ρ is the fluid density. Repeated computations are required for the same model using different grid divisions until the calculation results are almost equal.

2.3 Wind velocity reduction coefficient

For the main girder with wind barriers, there exists a boundary layer with a certain thickness

when lateral wind flows through the bridge deck, so the wind velocity u(z) at different heights from the bridge deck is different. To evaluate the windbreak effect of wind barriers, the equivalent wind velocity at the bridge deck is defined according to the equivalence theory of lateral aerodynamic force at the range of certain height (Guo *et al.* 2009). Based on this theory, and the wind pressure is proportional to u^2, the expression of equivalent wind velocity is as follows

$$\bar{u}_{\mathrm{eq}} = \sqrt{\frac{1}{z_{\mathrm{r}}}\int_0^{z_{\mathrm{r}}} u^2(z)\mathrm{d}z} \tag{17}$$

where z_{r} is the equivalent height in which the side wind affects the running train. For four types of train vehicles commonly used in China, the heights from rail surface to the top of car-body are, respectively, 4.433 m for passenger cars, 4.063 m for boxcars, 4.029 m for tank cars and 3.082 m for gondola cars. Thus, the height z_{r} in this study is taken as 5 m for passenger cars, boxcars and tank cars, and 4m for gondola cars. The wind velocity u(z) at different heights from the bridge deck can be obtained by the Fluent software computation.

The windbreak effect of wind barriers can be evaluated by a factor λ called wind velocity reduction coefficient, which is the ratio of the equivalent wind velocity at bridge deck to the oncoming wind velocity, i.e.

$$\lambda = \bar{u}_{\mathrm{eq}} / \bar{u} \tag{18}$$

where $\bar{u}$ is the oncoming wind velocity at the bridge deck.

2.4 Wind forces acting on bridge

The wind forces acting on the bridge include the static force caused by mean wind, the buffeting force caused by fluctuating wind, and the self-exciting force caused by the interaction between the wind and bridge motions. Each component contains forces from three directions of drag force, lift force and moment. The lift force L_{st}, drag force D_{st} and moment M_{st} per unit length caused by mean wind can be calculated according to the classical airfoil theory

$$L_{\mathrm{st}} = \frac{1}{2}\rho\bar{u}^2 C_{\mathrm{L}}(\alpha)B \tag{19a}$$

$$D_{\mathrm{st}} = \frac{1}{2}\rho\bar{u}^2 C_{\mathrm{D}}(\alpha)D \tag{19b}$$

$$M_{\mathrm{st}} = \frac{1}{2}\rho\bar{u}^2 C_{\mathrm{M}}(\alpha)B^2 \tag{19c}$$

where the subscript st represents the static forces; $C_{\mathrm{L}}(\alpha)$, $C_{\mathrm{D}}(\alpha)$ and $C_{\mathrm{M}}(\alpha)$ are, respectively, the lift, drag and moment coefficient, which are non-dimensional coefficients determined by the structure size and wind attack angle α, whose values can be measured from wind tunnel tests of section model; B and D are, respectively, the width and height of the bridge deck segment.

The buffeting forces per unit length are commonly expressed in terms of quasi-steady model as follows (Xia *et al*. 2011)

$$D_{\mathrm{bf}}(t) = \frac{1}{2}\rho\bar{u}^2 B\left[2\frac{D}{B}C_{\mathrm{D}}(\alpha)\frac{u(t)}{\bar{u}}\right] \tag{20a}$$

$$L_{\mathrm{bf}}(t)=\frac{1}{2}\rho\bar{u}^2B\left[2C_{\mathrm{L}}(\alpha)\frac{u(t)}{\bar{u}}+[C'_{\mathrm{L}}(\alpha)+\frac{D}{B}C_{\mathrm{D}}(\alpha)]\frac{w(t)}{\bar{u}}\right] \tag{20b}$$

$$M_{\mathrm{bf}}(t)=\frac{1}{2}\rho\bar{u}^2B^2\left[2C_{\mathrm{M}}(\alpha)\frac{u(t)}{\bar{u}}+C'_{\mathrm{M}}(\alpha)\frac{w(t)}{\bar{u}}\right] \tag{20c}$$

where the subscript bf represents the buffeting force; $C'_{\mathrm{D}}=\mathrm{d}C_{\mathrm{D}}/\mathrm{d}\alpha$, $C'_{\mathrm{L}}=\mathrm{d}C_{\mathrm{L}}/\mathrm{d}\alpha$, $C'_{\mathrm{M}}=\mathrm{d}C_{\mathrm{M}}/\mathrm{d}\alpha$; $u(t)$ and $w(t)$ are the lateral and vertical components of the fluctuating wind velocity, respectively.

The self-excited forces per unit length, i.e., lift $L_{\mathrm{se}}(t)$, drag $D_{\mathrm{se}}(t)$, and moment $M_{\mathrm{se}}(t)$ are commonly described utilizing flutter derivatives in frequency domain as follows (Chen *et al*. 2000)

$$L_{\mathrm{se}}(t)=\frac{1}{2}\rho\bar{u}^2B\left[KH_1^*(K)\frac{\dot{h}_{\mathrm{b}}}{\bar{u}}+KH_2^*(K)\frac{B\dot{\phi}_{\mathrm{b}}}{\bar{u}}+K^2H_3^*(K)\phi_{\mathrm{b}}+K^2H_4^*(K)\frac{h_{\mathrm{b}}}{B}+KH_5^*(K)\frac{\dot{p}_{\mathrm{b}}}{\bar{u}}+K^2H_6^*(K)\frac{p_{\mathrm{b}}}{B}\right] \tag{21a}$$

$$D_{\mathrm{se}}(t)=\frac{1}{2}\rho\bar{u}^2B\left[KP_1^*(K)\frac{\dot{p}_{\mathrm{b}}}{\bar{u}}+KP_2^*(K)\frac{B\dot{\phi}_{\mathrm{b}}}{\bar{u}}+K^2P_3^*(K)\phi_{\mathrm{b}}+K^2P_4^*(K)\frac{p_{\mathrm{b}}}{B}+KP_5^*(K)\frac{\dot{h}_{\mathrm{b}}}{\bar{u}}+K^2P_6^*(K)\frac{h_{\mathrm{b}}}{B}\right] \tag{21b}$$

$$M_{\mathrm{se}}(t)=\frac{1}{2}\rho\bar{u}^2B^2\left[KA_1^*(K)\frac{\dot{h}_{\mathrm{b}}}{\bar{u}}+KA_2^*(K)\frac{B\dot{\phi}_{\mathrm{b}}}{\bar{u}}+K^2A_3^*(K)\phi_{\mathrm{b}}+K^2A_4^*(K)\frac{h_{\mathrm{b}}}{B}+KA_5^*(K)\frac{\dot{p}_{\mathrm{b}}}{\bar{u}}+K^2A_6^*(K)\frac{p_{\mathrm{b}}}{B}\right] \tag{21c}$$

where the subscript se represents the self-excited wind forces; H_i^*, P_i^* and A_i^* ($i=1,\ldots,6$) are frequency dependent flutter derivatives from wind tunnel tests; $K=B\omega/\bar{u}$ is reduced frequency; ω is the circular frequency of vibration; h_{b}, p_{b}, and ϕ_{b} are vertical, lateral, and torsional displacement of bridge , respectively. The detailed process and method for the self-excited forces from frequency domain to time domain can be found in Xia *et al.* (2011).

2.5 Simulation of aerodynamic forces on train

Similar to the bridge, wind forces acting on a train in cross-wind field can be divided into two parts, i.e., the steady aerodynamic forces induced by the mean wind velocity component of natural wind and the unsteady aerodynamic forces induced by the fluctuating wind velocity component (Baker 1991). The wind forces acting on the bogie and wheel-sets of the vehicle are neglected because of their small windward area, thus only wind forces acting on the car-body are taken into account, which mainly refer to side force F_{S}, lift F_{L} and rolling moment M with respect to the mass center of the car body, as shown in Fig. 1.

If all the vehicles are the same in a train, the conventional strip theory and quasi-steady theory for bridge decks can be also used to calculate the aerodynamic forces on the train. From Fig. 1, the instantaneous wind velocity V and wind attack angle α can be written as

$$V^2=(\bar{u}+u)^2+w^2 \tag{22a}$$

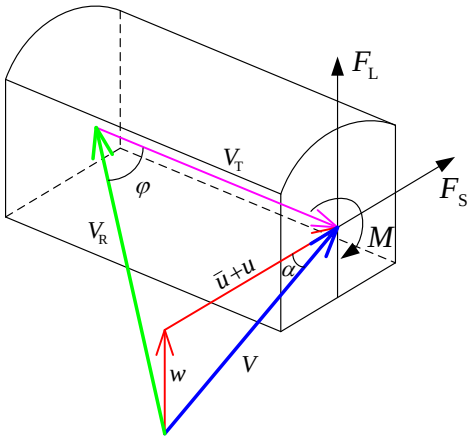

Fig. 1 Wind forces acting on the car-body of a train vehicle

$$\alpha = \arctan\frac{w}{\bar{u}+u} \tag{22b}$$

Suppose the train runs on a straight track at a constant speed V_T, the wind velocity V_R relative to the vehicle and its yaw angle φ can be expressed as

$$V_R^2 = V^2 + V_T^2 = \left[(\bar{u}+u)^2 + w^2\right] + V_T^2 \tag{23a}$$

$$\varphi = \arctan\left(\sqrt{(\bar{u}+u)^2 + w^2}\,/V_T\right) \tag{23b}$$

Generally, the lateral fluctuating wind velocity u and the vertical fluctuating wind velocity w are considerably smaller than the mean wind velocity $\bar{u}$, so the higher-order quantities such as u^2, w^2 and uw can be neglected, and Eqs. (22) and (23) can be simplified as

$$V^2 \approx \bar{u}^2 + 2\bar{u}u \qquad \alpha \approx \arctan\frac{w}{\bar{u}} \tag{24}$$

$$V_R^2 \approx (\bar{u}^2 + 2\bar{u}u) + V_T^2 \qquad \varphi \approx \arctan(\bar{u}/V_T) \tag{25}$$

According to quasi-steady theory, the aerodynamic forces on the running train can be expressed as

$$F_S = \frac{1}{2}\rho A V_R^2 C_{F_S}(\alpha,\varphi) \tag{26a}$$

$$F_L = \frac{1}{2}\rho A V_R^2 C_{F_L}(\alpha,\varphi) \tag{26b}$$

$$M = \frac{1}{2}\rho A V_R^2 H C_{Mv}(\alpha,\varphi) \tag{26c}$$

where A and H are the reference area and height of the vehicle, respectively; C_{F_S}, C_{F_L} and C_{M_V} are the aerodynamic coefficients of vehicle that are the function of wind attack α and yaw angle φ. Based on the Taylor series expansion at $\alpha=0$, these coefficients can be approximated as

$$C_i(\alpha,\varphi)=C_i(\varphi)+C_i'(\varphi)\cdot\alpha\approx C_i(\varphi)+C_i'(\varphi)\cdot\frac{w}{\bar{u}} \tag{27}$$

where $C_i(\varphi)$ and $C_i'(\varphi)$ $(i=F_S,F_L,M_v)$ are the side force, lift force and moment coefficients of the vehicle and their first order derivatives at $\alpha=0$.

Substituting Eqs. (24), (25) and (27) into Eq. (26), the wind forces acting on the car body can be given

$$F_S=0.5\rho A\bar{V}_R^2C_{F_S}(\varphi)+0.5\rho A\bar{V}_R^2\left[C_{F_S}(\varphi)\cdot\frac{2\bar{u}u}{\bar{V}_R^2}+C_{F_S}'(\varphi)\cdot\frac{w}{\bar{u}}\right] \tag{28a}$$

$$F_L=0.5\rho A\bar{V}_R^2C_{F_L}(\varphi)+0.5\rho A\bar{V}_R^2\left[C_{F_L}(\varphi).\frac{2\bar{u}u}{\bar{V}_R^2}+C_{F_L}'(\varphi).\frac{w}{\bar{u}}\right] \tag{28b}$$

$$M=0.5\rho A\bar{V}_R^2HC_{Mv}(\varphi)+0.5\rho A\bar{V}_R^2H\left[C_{Mv}(\varphi)\cdot\frac{2\bar{u}u}{\bar{V}_R^2}+C_{Mv}'(\varphi)\cdot\frac{w}{\bar{u}}\right] \tag{28c}$$

where $\bar{V}_R^2=V_T^2+\bar{u}^2$.

In the right side of Eq. (28), the first term represents the steady aerodynamic force, while the other two terms represent the unsteady, respectively. The aerodynamic admittance functions are often introduced to reduce the errors involved in quasi-steady theory for the unsteady aerodynamic forces as follows

$$F_S^{ust}=0.5\rho A\bar{V}_R^2\left[\chi_{F_{Su}}(f)\cdot C_{F_S}(\varphi)\cdot\frac{2\bar{u}u}{\bar{V}_R^2}+\chi_{F_{Sw}}(f)\cdot C_{F_S}'(\varphi)\cdot\frac{w}{\bar{u}}\right] \tag{29a}$$

$$F_L^{ust}=0.5\rho A\bar{V}_R^2\left[\chi_{F_{Lu}}(f)\cdot C_{F_L}(\varphi)\cdot\frac{2\bar{u}u}{\bar{V}_R^2}+\chi_{F_{Lw}}(f)\cdot C_{F_L}'(\varphi)\cdot\frac{w}{\bar{u}}\right] \tag{29b}$$

$$M^{ust}=0.5\rho A\bar{V}_R^2H\left[\chi_{M_u}(f)\cdot C_{Mv}(\varphi)\cdot\frac{2\bar{u}u}{\bar{V}_R^2}+\chi_{M_w}(f)\cdot C_{Mv}'(\varphi)\cdot\frac{w}{\bar{u}}\right] \tag{29c}$$

where the superscript ust represent the unsteady aerodynamic forces; $\chi_{F_{Su}}(f)$, $\chi_{F_{Sw}}(f)$, $\chi_{F_{Lu}}(f)$, $\chi_{F_{Lw}}(f)$, $\chi_{M_u}(f)$ and $\chi_{M_w}(f)$ are aerodynamic transfer functions between the fluctuating wind velocity and aerodynamic forces, and f is the frequency in Hz.

It can be seen from Eq. (29) that the fluctuating components of wind velocity field u and w should be obtained in order to decide the unsteady aerodynamic forces. In addition, the aerodynamic coefficients of the vehicle and their first order derivations, aerodynamic transfer functions also should be provided. Of course, the turbulent wind velocities can be simulated at a series of points along a longitudinal line passing through the mass center of the car-body by the method in Section 2.1. For lack of available data, all aerodynamic transfer functions are taken as

1.0 in calculation of the unsteady wind forces (Xu *et al.* 2006).

3. Dynamic model of vehicle-bridge system in wind field

The dynamic model of vehicle-bridge system in wind field is composed of three parts: the train subsystem, the bridge subsystem, and the wind loads acting on the train-bridge system.

The train subsystem consists of several locomotives and vehicles. Each locomotive or vehicle is composed of a car-body, bogies, wheel-sets, and the spring and dashpot connections between the three components.

For the bridge model using for vehicle-bridge dynamic analysis, it can be established by the finite element method or the modal decomposition technique according to the type of bridge structures.

The calculation procedure of the wind loads on the bridge and the train are described in Sections 2.4 and 2.5.

3.1 Modeling of vehicle

In this paper, a 4-axle vehicle with two suspension systems is taken as an example to demonstrate the modeling of the vehicle (see Fig. 2). To simplify the analysis but with enough accuracy, the following assumptions are used in the modeling the vehicle subsystem:

(i) The vehicle runs on the track at a constant speed V_T, so that it is unnecessary to model the movement of the car-body in the longitudinal direction.

(ii) The car-body, bogies and wheel-sets are regarded as rigid components, neglecting their elastic deformation during vibration.

(iii) The connections between a bogie and the wheel-sets are characterized by linear springs and viscous dashpots with identical properties, named the first suspension system. The connections between the car-body and the bogies are represented by linear springs and viscous dashpots of identical properties, named the secondary suspension system.

(iv) The wheel-set and rail keep contact, thus the movement of the wheel-set can be expressed by the bridge movement and the corresponding rail irregularity profile.

Both the car-body and each bogie have five degrees-of-freedom, including floating, lateral swing, rolling, yawing and pitching movements. Each wheel-set has three degrees-of-freedom, including floating, lateral swing and rolling movements with respect to its mass center. As a result, the total degrees-of-freedom for a four-axle vehicle are 27, as shown in Fig. 2.

3.2 Modeling of bridge

The bridge is composed of girders, piers, abutments, deck system and track system. Due to the complexity of coupled components, the following assumptions are adopted in modeling the bridge subsystem:

(i) There is no relative movement between the track and bridge deck, and the elastic deformation of the track system is neglected.

(ii) The girders and piers are modeled adopting spatial beam element, and the damping matrix is assumed as Rayleigh damping.

Based on the above assumptions, the bridge is discretized as a three-dimensional finite element model. By applying the modal decomposition technique where the generalized coordinates of

bridge vibration modes are solved rather than the motion equations of the bridge directly, the total number of the degrees-of-freedom of the system is significantly reduced and the coupled equations of motion are efficiently solved. Detailed formulations can be found in Guo *et al.* (2007).

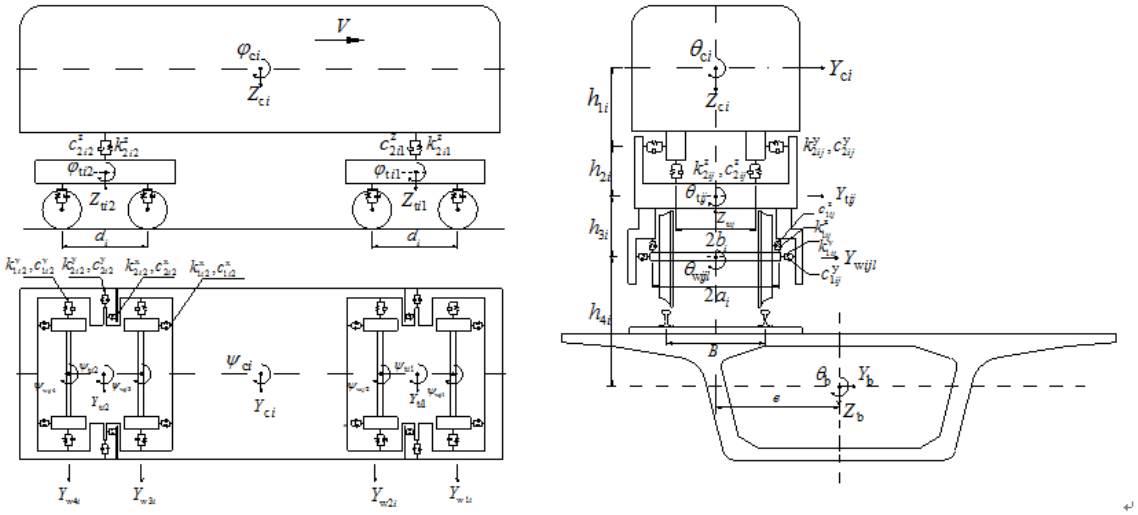

Fig. 2 Model of vehicle subsystem

3.3 Coupled vehicle-bridge system under cross winds

According to the train submodel, the bridge submodel, the assumed train-bridge interaction relationship, and the wind forces acting on the train and bridge described above, the equations of motion of the train-bridge coupled system under wind action can be expressed as

$$\begin{bmatrix} \mathbf{M}_{vv} & \mathbf{0} \\ \mathbf{0} & \mathbf{M}_{bb} \end{bmatrix} \begin{Bmatrix} \ddot{\mathbf{X}}_v \\ \ddot{\mathbf{X}}_b \end{Bmatrix} + \begin{bmatrix} \mathbf{C}_{vv} & \mathbf{C}_{vb} \\ \mathbf{C}_{bv} & \mathbf{C}_{bb} \end{bmatrix} \begin{Bmatrix} \dot{\mathbf{X}}_v \\ \dot{\mathbf{X}}_b \end{Bmatrix} + \begin{bmatrix} \mathbf{K}_{vv} & \mathbf{K}_{vb} \\ \mathbf{K}_{bv} & \mathbf{K}_{bb} \end{bmatrix} \begin{Bmatrix} \mathbf{X}_v \\ \mathbf{X}_b \end{Bmatrix} = \begin{Bmatrix} \mathbf{F}_{v0} \\ \mathbf{F}_{b0} \end{Bmatrix} + \begin{Bmatrix} \mathbf{F}_v^{st} + \mathbf{F}_v^{ust} \\ \tilde{\mathbf{F}}_b^{st} + \tilde{\mathbf{F}}_b^{bf} + \tilde{\mathbf{F}}_b^{se} \end{Bmatrix} \tag{30}$$

where: $\mathbf{M}_{vv}$, $\mathbf{C}_{vv}$ and $\mathbf{K}_{vv}$ are the mass, damping and stiffness matrices of the train; $\mathbf{M}_{bb}$, $\mathbf{C}_{bb}$ and $\mathbf{K}_{bb}$ are the mass, damping and stiffness matrices of the bridge; $\mathbf{K}_{vb}$ and $\mathbf{K}_{bv}$, $\mathbf{C}_{vb}$ and $\mathbf{C}_{bv}$ are the stiffness and damping matrices due to the interaction between the bridge and the train; $\mathbf{X}_v$, $\dot{\mathbf{X}}_v$, $\ddot{\mathbf{X}}_v$ and $\mathbf{X}_b$, $\dot{\mathbf{X}}_b$, $\ddot{\mathbf{X}}_b$ are the displacement, velocity and acceleration vectors of the train and the generalized coordinate vector of the bridge; $\mathbf{F}_{v0}$ and $\mathbf{F}_{b0}$ are the force vectors due to the train-bridge interaction through the track and wheels; $\tilde{\mathbf{F}}_b^{st}$, $\tilde{\mathbf{F}}_b^{bf}$, and $\tilde{\mathbf{F}}_b^{se}$ are the modal static wind force vector, buffeting force vector and the self-excited force vector of the bridge; and $\mathbf{F}_v^{st}$ and $\mathbf{F}_v^{ust}$ are the steady force vector and unsteady force vector of the vehicle, respectively.

Eq. (30) is actually the second order linear non-homogeneous differential equation with time-varying coefficients, which can be solved using the *Newmark-β* implicit integral algorithm or other numerical methods.

4. Case study

4.1 Background

The total length of the new-built second double-line railway from Lanzhou to Xinjiang is about 1780 km, which will be the longest high-speed railway line in China. The design train speed is 200 km/h. The wind environment is very serious along the railway line. There exist some strong windy zones such as the Anxi windy zone in Gansu, the Yandun windy zone, the 50-km windy zone, and the Dabancheng windy zone in Xinjiang, with the total length of about 330 km. The airflows with the characteristic of sand-driving wind in the region, the wind velocity is high, and the destructive power is strong. In addition to the serious train operation accidents caused by strong wind, there are many other problems such as the breakage of window of the vehicle, cement hardening, rail wears, and shortened service life of technical equipments for train safety. Therefore, it is indispensable to analyze the running safety of high-speed train and the windbreak measures, to ensure the operation safety of railway bridges in this strong wind field.

In this case study, the distribution law of wind velocity along the height above the bridge deck is studied for the bridge with simply-supported box-girders on the new Lanzhou-Xinjiang railway. The bridge is installed with wind barriers with different porosity rates and heights, as shown in Fig. 3.

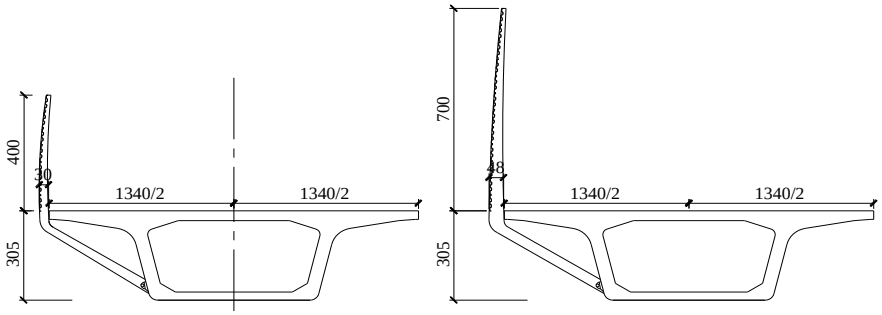

(a) Cross sections of wind barriers with different heights

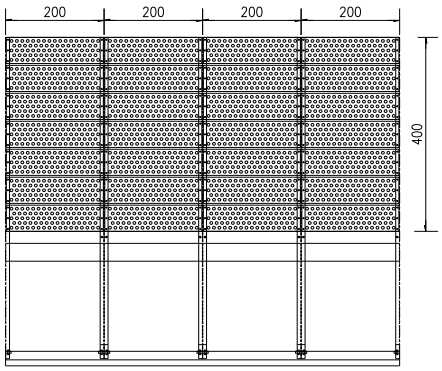

(b) Elevation of the single-side wind barrier (4 m high)

Fig. 3 Single-side wind barriers on the box-girder (Unit: cm)

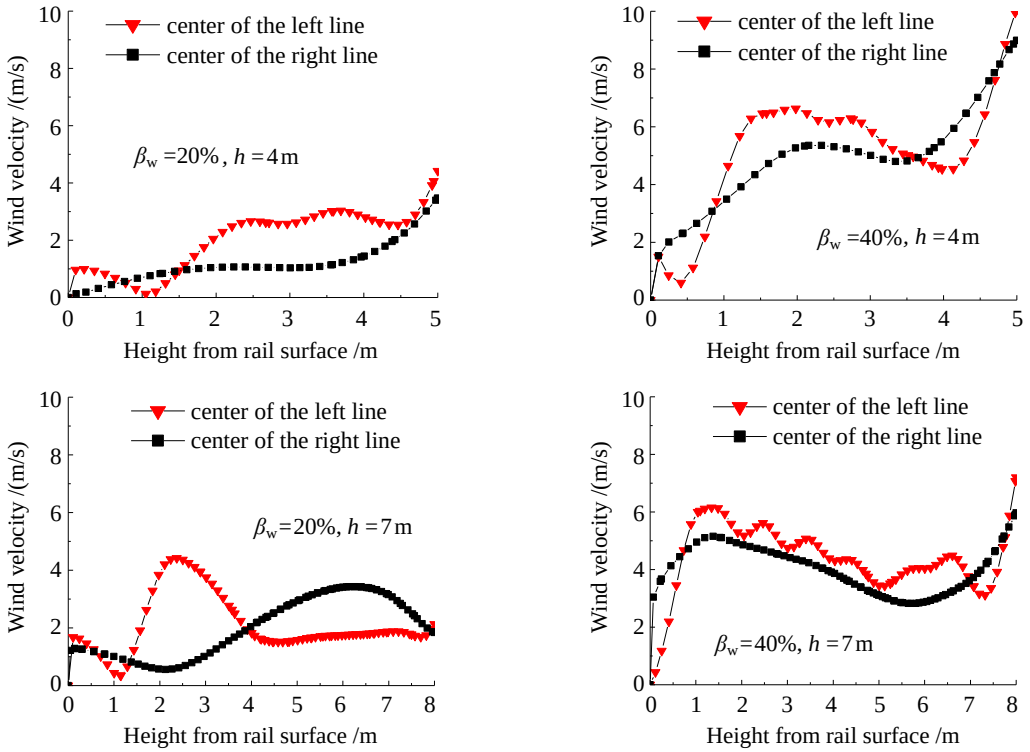

Fig. 4 Wind velocity distributions along the height at the track central line on the box-girder with wind barriers

The wind velocity reduction coefficients are calculated to select the proper type of wind barriers. Then the dynamic response of the bridge and the running safety indices of the train are calculated in cases with and without wind barriers when the wind acts at the level of the vehicle mass center in the direction normal to the motion of the vehicle.

4.2 Comparison of windbreak effect for wind barriers

The form selection for wind barriers are based on these cases: the barrier height is 4 m and 7 m, the porosity rate β_w is 10%, 20%, 30%, 40% and 50%, which is the ratio of the hole area to the whole area per unit length of the wind barrier. The numerical simulation is carried using the FLUENT software for all cases. The wind attack angle is zero degree, the oncoming wind velocity is 10 m/s, the structure surface and the upper and lower surface of the computation region are the wall conditions, the velocity condition for the inlet boundary condition, and the pressure boundary condition for the outlet boundary condition.

Illustrated in Fig. 4 are the distribution curves of wind velocity along the height at the track central line on the box-girder with wind barriers of different porosity rates.

It is clearly shown that the wind barriers can effectively reduce the wind velocity on the bridge deck, and the windbreak effect is closely related to the porosity rate and height of barriers. The wind velocity in the protection region increases with the porosity rate β_w. In general, the wind

Table 1 Wind velocity reduction coefficients of wind barriers with different porosity rates

Porosity rate	4 m high single-side wind barrier		7m high single-side wind barrier	
	At the center of the left line	At the center of the right line	At the center of the left line	At the center of the right line
10%	0.103	0.116	0.224	0.196
20%	0.219	0.126	0.262	0.145
30%	0.387	0.298	0.357	0.295
40%	0.535	0.498	0.476	0.431
50%	0.585	0.585	0.527	0.482

velocity at the left line is bigger than that at the right line, and it presents a waving form due to the influence of holes at the left line position close to wind barriers. At the height range of 4 m from rail surface, the difference in wind velocity using 4 m or 7 m wind barriers is not so big, but the wind velocity above 4 m obviously increase for 4 m single-side wind barrier. The turbulent intensity is significantly reduced, so hereinafter only the steady forces acting on the vehicle are calculated for the bridge installed with wind barriers, while for bridge without wind barriers, both the steady forces and unsteady forces on the vehicle are taken into account.

Based on the theory in Section 2.3, the wind velocity reduction coefficients are calculated for different porosity rates and heights of wind barriers as $z_r=5$m, as shown in Table 1. It can be seen that the wind velocity reduction coefficient for the 4 m wind barrier is smaller than that for the 7 m wind barrier when the porosity rate is not bigger than 20%. The windbreak effect for the 7 m wind barrier is better than that for the 4 m barrier when the rate is greater or equal to 30%. Therefore, at the range of 5 m protection height, the 4 m single-side wind barrier with the porosity rate about 20% is a reasonable form to protect the train operation, which can reduce the wind velocity at the rail central line by about 80%. This type of wind barrier is used on the bridge in the dynamic analysis of coupled wind-vehicle-bridge system.

4.3 Train parameters and finite element model of bridge

The train used for the case study is the ICE train in Germany, composed of 3×(3M+1T), where M represents the motor-car and T the trailer-car. The height and width of the car-body are 3.5 m and 2.7 m, respectively. The average static axle load is 160 kN for a motor-car and 146 kN for a trailer car. The other parameters of the ICE train can be found in Xia *et al.* (2011).

The track vertical, lateral, and torsional irregularities are generated from the German PSD functions of rail irregularities for high-speed railway, which are recommended by the technical condition of the high-speed train in China (Xia *et al.* 2011). The length of the simulated data is 2000 m with the maximum amplitude being 4.20 mm in the lateral direction, 5.80 mm in the vertical direction and 0.002 rad in the torsional direction, as shown in Fig. 5.

The bridge consists of 10×32 m simply-supported box-girders with 13.4 m width, and the solid piers of 15 m height. The bridge model established with finite elements is shown in Fig. 6. The range of natural frequency of the first 60 orders is from 1.23 Hz to 27.1 Hz.

4.4 Wind loads

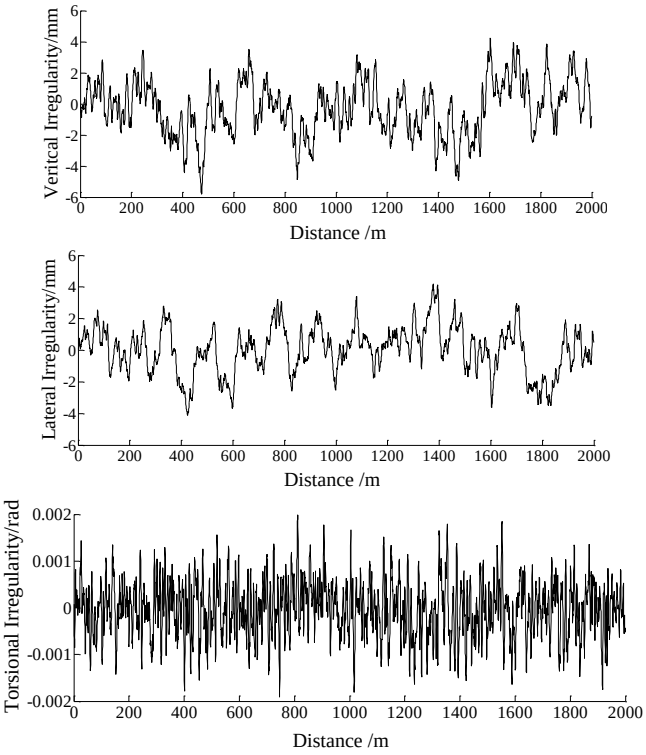

Fig. 5 Simulated track irregularities in the case study

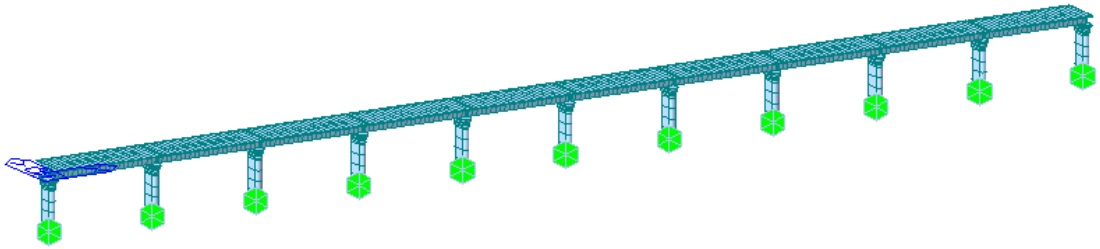

Fig. 6 Finite element model of the bridge

The fluctuating wind velocity time histories at the bridge site are simulated to calculate the buffeting forces on the bridge and the unsteady aerodynamic forces on the train without wind barriers. The following lateral and vertical wind auto-spectra are adopted in the code of China (JTG/T D60-01-2004)

$$\frac{fS_u(f)}{u_*^2} = \frac{200 f_*}{(1+50 f_*)^{5/3}} \tag{31}$$

$$\frac{fS_w(f)}{u_*^2} = \frac{6 f_*}{(1+4 f_*)^2} \tag{32}$$

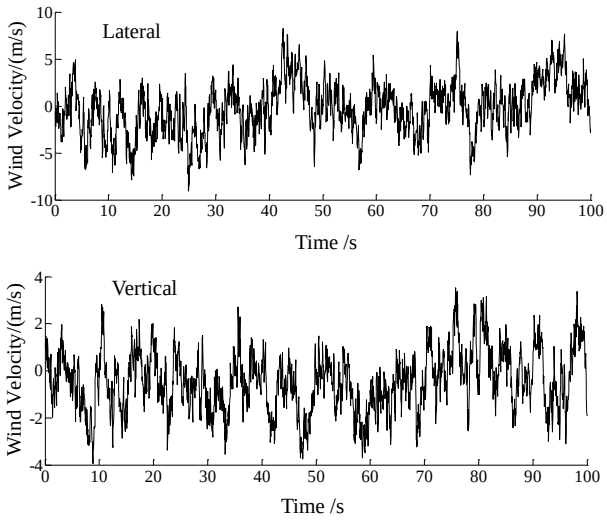

Fig. 7 Simulated fluctuating wind velocity time histories

Table 2 Aerodynamic coefficient

Item	C_{D}	C_{L}	C_{M}	C'_{L}	C'_{M}
Bridge without wind barriers	1.0903	0.4681	0.1483	0.7391	-0.4011
Vehicle on the bridge without wind barriers	1.37	0.0524	0.82	--	--
Bridge with 4m high wind barriers	2.0302	-0.1334	0.2366	0.0573	0.1318
Vehicle on the bridge with 4m high wind barriers	0.329	0.094	0.212	--	--

where $f_* = \dfrac{fz}{\bar{u}(z)}, u_* = \dfrac{K\bar{u}(z)}{\mathrm{In}[(z-z_{\mathrm{d}})/z_0]}, z_{\mathrm{d}} = \bar{H} - z_0/K$; $S_u(f)$ and $S_w(f)$ are, respectively, the power spectral density functions in the lateral and vertical direction; u_* is the friction velocity of the airflow, in m/s; K is a non-dimensional const, $K \approx 0.4$; z is the height from ground or water surface, in m; $\bar{u}(z)$ is the mean wind velocity at the height z, in m/s; z_0 is the ground roughness height, in m; $\bar{H}$ is the mean height of surrounding buildings.

Fig. 7 shows the time histories of vertical and lateral fluctuating wind velocity at a point of the bridge, corresponding to the mean wind velocity 25 m/s.

For simulation of dynamic behaviors of the train-bridge system under crosswinds, the aerodynamic data, including both steady force coefficients and turbulent characteristics, for the bridge and the moving train are required. These values can be acquired from a wind tunnel experiment. The aerodynamic coefficients of the bridge and their first derivatives at the zero wind attack angle are listed in Table 2, also the aerodynamic coefficients of the vehicle at zero the wind attack angle and 90° yaw angle. Thus, the wind forces on the bridge and vehicle can be easily calculated using the method described above.

4.5 Bridge response with wind barriers

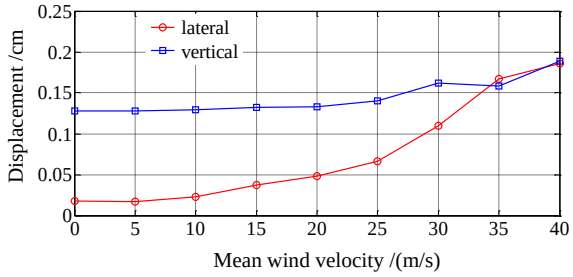

(a) *vs.* mean wind velocity as $V_T = 200$ km/h

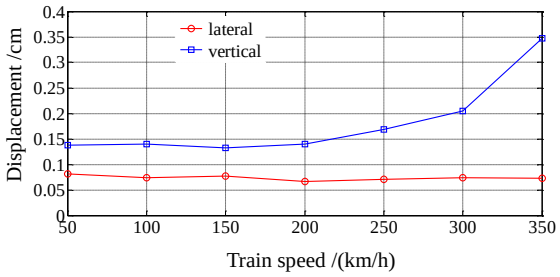

(b) *vs.* train speed as $\bar{u} = 25$ m/s

Fig. 8 Maximum displacements of the bridge

The maximum displacement responses of the bridge versus mean wind velocity are plotted in Fig. 8(a), where the train speed is 200 km/h, and those versus train speed are in Fig. 8(b), where the wind velocity is 25 m/s. It can be seen that wind force has obvious influence on the lateral displacement of the bridge, which is very small without wind action but increases significantly with the wind velocity. The train speed has small effect on the lateral displacement of the bridge, but great effect on the vertical displacement of the bridge, especially when the train speed is higher than 200 km/h. This is because the vertical displacement of the bridge is mainly caused by the moving gravity force of the train, while the lateral displacement is mainly caused by the wind forces.

Fig. 9 shows the time histories of lateral and vertical accelerations of the bridge, when the train runs at 200 km/h on the sixth span without and with wind forces. The time histories show that the accelerations reach the maximum value when the train travels on the bridge, while the fluctuating wind forces have slight effect, because the accelerations are mainly caused by the track irregularity and train excitation. The accelerations decrease rapidly after the train leaves the span without wind action, while they obviously have turbulent characteristic with wind action. The maximum mid-span accelerations of the sixth span are, respectively, 15.3 cm/s^2 without wind and 19.5 cm/s^2 with wind in lateral direction, and 15.2 cm/s^2 without wind and 14.6 cm/s^2 with wind in vertical direction.

4.6 Vehicle response and safety indices with wind barriers

The evaluation indices for the running safety of train currently adopted in the high-speed railways in China include: the derailment factor Q/P_1(defined as the ratio of the lateral wheel-rail force Q to the vertical force P_1 of the wheel at the climbing-up-rail side), the offload factor $\Delta P / \bar{P}$

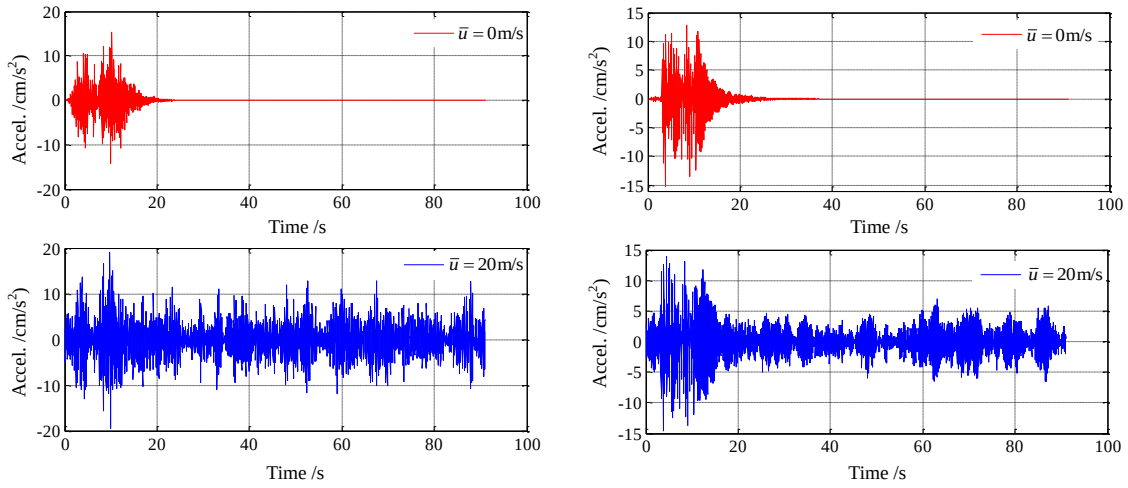

(a) Lateral (b) Vertical

Fig. 9 Mid-span acceleration time histories of the sixth span of the bridge as V_T = 200 km/h

Table 3 Maximum dynamic response of the train with wind barriers (V_T = 200 km/h)

Wind velocity $\bar{u}$ /(m/s)			0	5	10	15	20	25
Acceleration of car-body /(cm/s^2)	Vertical	motor-car	63.5	63.5	63.5	63.5	63.5	63.51
		trailer-car	46.34	46.34	46.27	46.39	46.38	46.92
	Lateral	motor-car	51.32	51.37	51.49	51.98	52.79	54.53
		trailer-car	59.72	59.73	59.77	59.85	59.93	60.07
Offload factor		motor-car	0.193	0.195	0.229	0.297	0.402	0.545
		trailer-car	0.157	0.157	0.201	0.282	0.408	0.575
Derailment factor		motor-car	0.209	0.218	0.249	0.306	0.400	0.574
		trailer-car	0.241	0.232	0.224	0.281	0.404	0.666
Lateral W/R force /kN		motor-car	32.5	33.6	37.0	42.5	50.0	60.3
		trailer-car	30.6	29.8	33.1	38.5	46.2	56.0

(defined as the ratio of the offload vertical wheel-rail force ΔP to the average vertical wheel-rail force $\bar{P}$ of the two wheels on a wheel-set), and the lateral wheel-rail force H.

The maximum acceleration responses and running safety indices of the train vehicles, such as offload factor, derailment factor and lateral wheel-rail force, are listed in Table 3, as the train runs at 200 km/h and the mean wind velocity from 0 m/s to 25 m/s.

As can be seen, wind forces have slight effect on the accelerations of the car-body due to the wind barriers when the mean wind velocity is below 25 m/s. It is also shown that the offload factor and the derailment factor of the train under wind force are larger than those without wind force. These two factors increase with the mean wind velocity, and the greater the wind velocity is, the faster the increase growth, and this is similar to the lateral wheel-rail force. The maximum values of offload factor and derailment factor are 0.575 and 0.666, respectively, and the maximum lateral wheel-rail forces are 60.3 kN for the motor-car and 56.0 kN for the trailer-car, respectively, when the mean wind velocity reaches 25 m/s.

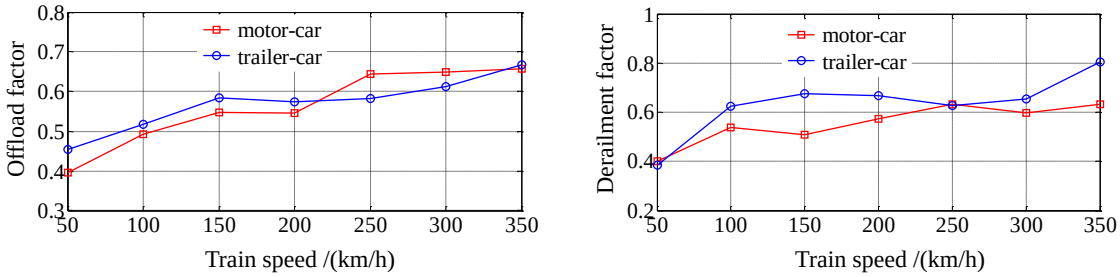

Fig. 10 Maximum offload factor and derailment factor *vs.* train speed ($\bar{u} = 25\,\mathrm{m/s}$)

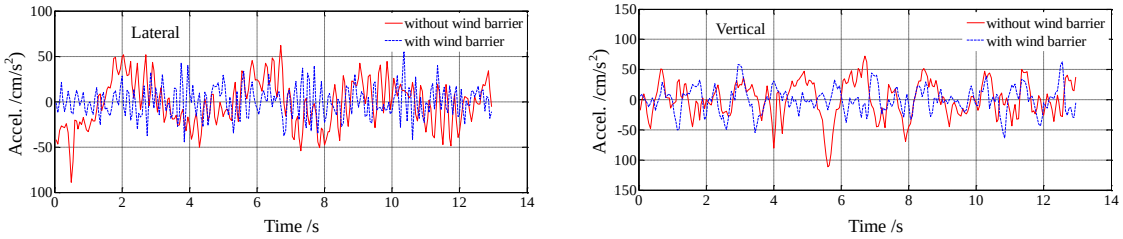

Fig. 11 Maximum acceleration time histories of the vehicle as V_T=200 km/h and $\bar{u} = 25\,\mathrm{m/s}$

Table 4 Maximum dynamic response of the train without wind barriers (V_T=200 km/h)

Mean wind velocity /(m/s)	Derailment factor	Offload factor	Lateral wheel-rail force / kN	Lateral acceleration of the car-body / (cm/s^2)	Vertical acceleration of the car-body / (cm/s^2)
0	0.24	0.19	32.5	59.7	63.5
5	0.26	0.25	37.1	59.3	63.7
10	0.48	0.51	50.8	59.9	64.0
15	2.5	0.99	74.1	64.5	70.0

Shown in Fig. 10 are, respectively, the distributions of offload factor and derailment factor of the train versus train speed while keeping the other parameters unchanged. It is seen that in general trend these factors increase with the train speed.

4.7 Vehicle response and safety indices without wind barriers

To investigate the windbreak effect of wind barrier, the car-body accelerations and running safety indices of the train are compared when it travels on the bridge without wind barriers. Fig. 11 shows the maximum acceleration time histories of the car-body in these two cases when the train speed is 200 km/h and the mean wind velocity is 25 m/s. With wind barriers, the maximum lateral acceleration is reduced from 88.9 cm/s^2 to 60.1 cm/s^2, and the vertical acceleration from 111.4 cm/s^2 to 63.5 cm/s^2.

The maximum responses of the train are listed in Table 4 without wind barriers as the train runs at the speed of 200 km/h increased the mean wind velocity to 15 m/s from 0 m/s. It can be seen that the derailment factor, offload factor and lateral wheel-rail force increase rapidly with the mean

Table 5 Limit train speeds with and without wind barriers

Mean wind velocity / (m/s)	Limit value of train speed / (km/h)		Mean wind velocity / (m/s)	Limit value of train speed / (km/h)	
	with barrier	without barrier		with barrier	without barrier
0	360	360	22.5	280	--
5	350	300	25	200	--
10	350	200	27.5	80	--
12.5	350	40	30	60	--
15	350	Forbidden running	32.5	30	--
20	350	--	>32.5	Forbidden running	--

wind velocity, especially when the wind velocity exceeds 10 m/s. The car-body acceleration is influenced little when the mean wind velocity is less than 10 m/s, and the difference is small with or without wind barriers (compare the results in Table 3 and Table 4). This indicates that the wind forces are not the main influence factor on car-body acceleration when the mean velocity is less than 10 m/s.

4.8 Limit value of train speed

In order to judge the running safety of the train, the allowances of these safety indices defined in Section 4.6 are given in the Chinese code (TB 10621-2009) as follows

$$\begin{aligned} &\text{Derailment factor:} && Q/P_1 \le 0.8 \\ &\text{Offload factor:} && \Delta P/\bar{P} \le 0.6 \\ &\text{Wheel/ rail force:} && H \le 10 + P_{st}/3 \end{aligned} \tag{33}$$

where, P_{st} denotes the static wheel-set load in kN. The allowable lateral wheel-rail forces for the motor-car and trailer-car of the train are, respectively, 63.3 kN and 58.7 kN, corresponding to their static loads 160 kN and 146 kN.

The allowances for the car-body accelerations in the Chinese code are as follows

$$\text{Vertical acceleration} \le 0.13g \tag{34a}$$

$$\text{Lateral acceleration} \le 0.10g \tag{34b}$$

Then the calculation results considering different wind velocities from 0 m/s to 32.5 m/s and train speeds from 30 km/h to 360 km/h are compared with the above allowances. The limit train speeds for running safety corresponding to different wind velocities are listed in Table 5.

One can find that, the limit values of train speed with respect to different wind velocities are raised obviously with wind barriers. When the mean wind velocity reaches 30 m/s, the train still runs safely on the bridge at the speed of 60 km/h. While for a bridge without wind barriers, it should be closed to the train when the mean wind velocity exceeds 12.5 m/s. Therefore, installing wind barriers on the bridge is an effective measure to reduce the number of stopping train operation in wind areas and to enhance the running safety of the train in wind field.

5 Conclusions

For the running safety of the train under cross winds, the wind barriers are installed on the bridge to reduce the wind forces acting on the vehicle. The form of wind barriers is selected based on the numerical simulation of airflow through wind barriers on bridge. A case study is performed to calculate the dynamic response of the bridge and the running safety indices of train on the bridge with and without wind barriers under cross winds. Some conclusions drawn from the study are as follows:

(1) The windbreak effect is closely related to the porosity rate and height of barriers. The wind barriers are suggested to have a height similar to the structures to be protected, and the porosity rate can be from 10% to 20%.

(2) Wind action has influence on the displacement responses of the bridge. The lateral displacement is very small without wind action but increases significantly with wind velocity. Train speed has small effect on the lateral displacement of the bridge, but great effect on the vertical displacement of the bridge, especially for train speed above 200 km/h.

(3) The fluctuating wind intensifies the acceleration of the bridge, and produces greater impact on lateral direction than on vertical direction. For a bridge without wind barriers, wind has strong influence on the acceleration of car-body when the mean wind velocity is higher than 10 m/s, while for a bridge with wind barriers, this influence is very slight when the wind velocity is below 25 m/s.

(4) The offload factor, derailment factor and lateral wheel-rail force of the train under cross wind increase with the wind velocity and the greater the wind velocity, the faster the increase rate. The increasing amplitude without wind barriers is much bigger than that with wind barriers.

(5) Installing wind barriers on the bridge can greatly raise the safety running speed of the train. For the bridge with a 4m high single-side wind barrier, the allowable wind velocity is 32.5 m/s, which is much greater than 12.5 m/s for the bridge without wind barriers.

Acknowledgements

The research described in this paper is supported by the Major State Basic Research Development Program of China (“973” Program: 2013CB036203), and the Fundamental Research Funds for the Central Universities of China (No.2013YJS054, No.2012JBM075).

References

Ahmed, S.R., Gawthorpe, R.G. and Mackrodt, P.A. (1985), “Aerodynamics of road and rail vehicles”, *Veh. Syst. Dyn.*, **14**(4-6), 319-392.

Andersson, E., Haggstrom, J., Sima, M. and Stichel, S. (2004), “Assessment of train-overturning risk due to strong cross-winds”, *J. Rail. Rap. Trans.*, **218**(3), 213-223.

Baker, C.J. (1991), “Ground vehicles in high cross winds part 1: steady aerodynamic forces”, *J. Fluids. Struct.*, **5**(2), 69-90.

Baker, C.J. (1991), “Ground vehicles in high cross winds part 2: unsteady aerodynamic forces”, *J. Fluids. Struct.*, **5**(2), 91-111.

Baker, C.J. and Reynolds, S. (1992), “Wind-induced accidents of road vehicles”, *Accid. Anal. Prev.*, **24**(6), 559-575.

Carrarini, A. (2007), "Reliability based analysis of the crosswind stability of railway vehicles", *J. Wind Eng. Ind. Aerod.*, **95**(7), 493-509.
Cheli, F., Corradi, R., Diana, G. and Tomasini, G. (2003), "A numerical-experimental approach to evaluate the aerodynamic effects on rail vehicle dynamics", *Veh. Syst. Dyn.*, **41**, 707-716.
Chen, R.L., Zeng, Q.Y., Huang, Y.Q., Xiang, J., Wen, Y., Guo, X.G., Yin, C.J., Dong, H. and Zhao, G. (2010), "Analysis theory of random energy of train derailment in wind", *Sci. Chin.* (*Phys., Mech. Astron.*), **53**(4), 751-757.
Chen, X.Z., Matsumoto, M. and Kareem, A. (2000), "Time domain flutter and buffeting response analysis of bridges", *J. Eng. Mech.*, **126**(1), 7-16.
Cooper, R.K. (1981), "The effect of cross winds on trains", *J. Fluid Mech.*, **103**(1), 170-178.
Cooper, R.K. (1979), "The probability of trains overturning in high winds", *Proceedings of the 5th International Conference on Wind Engineering*, Fort Collins, July.
Davenport, A.G. (1961), "The application of statistical concepts to the wind loading of structures", *Proc. Inst. Civ. Eng.*, **19**(2), 449-472.
Diedrichs, B. (2010), "Aerodynamic crosswind stability of a regional train model", *J. Rail. Rap. Tran.*, **224**(F6), 580-591.
Diedrichs, B., Sima1, M., Orellano, A. and Tengstrand, H. (2007), "Crosswind stability of a high-speed train on a high embankment", *J. Rail. Rap. Tran.*, **221**(2), 205-225.
Fujii, T., Maeda, T., Ishida, H., Imai, T., Tanemoto, K. and Suzuki, M. (1999), "Wind-induced accidents of train/vehicles and their measures in Japan", *Quart. Report Railway Tech. Res. Inst.*, **40**(1), 50-55.
Guo, W.W., Xu, Y.L., Xia, H., Zhang, W.S. and Shum, K.M. (2007), "Dynamic response of suspension bridge to typhoon and trains II: numerical results", *J. Struct. Eng.*, **133**(1), 12-21.
Guo, Z.S., Zhu, L.D. and Zhou, Z.Y. (2009), "Optimization selection of bridge windbreak and the influence on the aerodynamic performance of bridge", *Proceedings of the 14th Structural Wind Engineering Conference in China*, Beijng, September. (in Chinese)
Hagen, L.J., Skidmore, E.L., Miller, P.L. and Kipp, J.E. (1981), "Simulation of effect of wind barriers on airflow", *Transact. ASAE*, **24**(4), 1002-1008.
Han, Y., Chen, Z.Q. and Hua, X.G. (2010), "New estimation methodology of six complex aerodynamic admittance functions", *Wind Struct.*, **13**(3), 293-307.
Heisler, G.M. and Dewalle, D.R. (1988), "Effects of windbreak structure on wind flow", *Agric. Ecosystems Environ.*, **22/23**, 41-69.
Howell, J.P. (1986), "Aerodynamic response of maglev train models to a crosswind gust", *J. Wind Eng. Ind. Aerod.*, **22**(2-3), 205-213.
Kim, D.H., Kwon, S.D., Lee, I.K. and Jo, B.W. (2011), "Design criteria of wind barriers for traffic. Part 2: decision making process", *Wind Struct.*, **14**(1), 71-80.
Kwon, S.D., Kim, D.H., Lee, S.H. and Song, H.S. (2011), "Design criteria of wind barriers for traffic. Part 1: wind barrier performance", *Wind Struct.*, **14**(1), 55-70.
Liu, Q.K., Du, Y.L. and Qiao, F.G. (2008), "Train crosswind and strong wind countermeasure research in Japan", *J. Chin. Rail. Soc.*, **30**(1), 82-88. (in Chinese)
Li, X.Z. and Zhu, Y. (2010), "Stochastic space vibration analysis of a train-bridge coupling system", *Interact. Multiscale Mech.*, **3**(4), 333-342.
Li, Y.L., Qiang, S.Z., Liao, H.L. and Xu, Y.L. (2005), "Dynamics of wind-rail vehicle-bridge systems", *J. Wind Eng. Ind. Aerod.*, **93**(6), 483-507.
Ministry of Communications of PRC (2004), *Wind resistant design specification for highway bridges JTG/T D60-01-2004*, 46-47, China Communications Press, Beijing.
Ministry of Railways of PRC (2010), *Code for design of high-speed railway TB 10621-2009*, 58-59, China Railway Publishing House, Beijing.
Nikitas, N., Macdonald, J.H.G. and Jakobsen, J.B. (2011), "Identification of flutter derivatives from full-scale ambient vibration measurements of the Clifton Suspension Bridge", *Wind Struct.*, **14**(3), 221-238.
Noguchi, T. and Fujii, T. (2000), "Minimizing the effect of natural disasters", *Jpn. Rail. Transport Rev.*, **23**,

52-59.
Orellano, A., Schober, M. and BuXmann, C. (2002), "On side-wind stability of high-speed trains", *Proceedings of the 5th World Congress on Computational Mechanics*, Vienna, July.
Procino, L., Kozmar, H., Bartoli, G. and Borsani, A. (2008), "Wind barriers on bridges: the effect of wall porosity", *Proceedings of the 6th International Colloquium on*: *Bluff Bodies Aerodynamics & Application*s, Milano, July.
Qu, W.L. and Liu, L.N. (2007), "CFD-based numerical research in the identifying of tri-component force coefficient of bridge", *J. Wuhan Univ. Tech.*, **29**(7), 85-88.
Qian, Z.Y. (2009), "Strong wind disaster and control countermeasure for northwest China railways", *Chin. Rail*., **51**(3), 1-4. (in Chinese)
Saito, H., Suzuki, M. and Tanemoto, M. (2006), "Effects of wind fences on aerodynamic characteristics of train/ vehicles in cross winds", *Proceedings of the 6th Asia-Pacific Conference on Wind Engineering*, Seoul.
Simiu, E. and Scanlan, R.H. (1978), *Wind effects on structures*: *an introduction to wind engineering*, Wiley, New York.
Strukelj, A., Ciglaric, I. and Pipenbaher, M. (2005), "Analysis of a bridge structure and its wind barrier under wind loads", *Struct. Eng. Int.*, **15**(4), 220-227.
Suzuki, M., Tanemoto, K. and Maeda, T. (2003), "Aerodynamic characteristics of train/vehicles under cross winds", *J. Wind Eng. Ind. Aerod*., **91**(1), 209-218.
Wetzel, C. and Proppe, C. (2008), "Crosswind stability of high-speed trains: a stochastic approach", *Proceedings of the 6th International Colloquium on*: *Bluff Bodies Aerodynamics & Application*s, Milano, July.
Wilson, J.D. (1985), "Numerical studies of flow through a windbreak", *J. Wind Eng. Ind. Aerod*., **21**(2), 119-154.
Xia, H., Roeck, G.D. and Goicolea, J.M. (2011), *Bridge vibration and controls*: *New Research*, Nova Science Publishers, New York.
Xiang, H.F., Ge, Y.J., Zhu, L.D., Chen A.R., Gu, M. and Xiao, R.C. (2005), *Modern theory and practice on bridge wind resistance*, China Communications Press, Beijing.
Xu, Y.L. and Ding, Q.S. (2006), "Interaction of railway vehicles with track in cross-winds", *J. Fluids. Struct.*, **22**(3), 295-314.
Zhang, T., Xia, H. and Guo, W.W. (2012), "Simulation of bridge stochastic wind field using multi-variate auto-regressive model", *J. Cent. South Univ. (Sci. Tech.)*, **43**(3), 1114-1121. (in Chinese)
Zhang, W.M., Ge, Y.J. and Levitan, M.L. (2011), "Aerodynamic flutter analysis of a new suspension bridge with double main spans", *Wind Struct.*, **14**(3), 187-208.
Zhang, X.J. (2011), "Investigation on the wind-induced instability of long-span suspension bridges with 3D cable system", *Wind Struct.*, **14**(3), 209-220.
Zhou, Y. (2010), "Renormalization group theory for fluid and plasma turbulence", *Phys. Rep*., **488**(1), 1-49.

CC